Electronic Materials Letters, Vol. 4, No. 1 (2008), pp. 13-18

Effect of Cu Content on the Photovoltaic Properties of $Cu(In,Ga)Se_2$ Solar Cells Prepared by the Evaporation of Binary Selenide Sources

Doo Youl Lee, Min Sik Kim, Liudmila Larina, and Byung Tae Ahn*

Department of Material Science and Engineering, Korea Advanced Institute of Science and Technology, 335 Gwahangno, Yuseong-gu, Daejeon 305-701, Korea

A $Cu(In,Ga)Se_2$ light-absorbing layer was prepared by a three-stage process employing the evaporation of In_2Se_3, Ga_2Se_3, and Cu_2Se. The Cu content in the layer was adjusted by controlling the third-stage evaporation time. A sturdy n-CdS/p-CIGS junction was realized when the Cu content in $Cu_x(In_{0.66}Ga_{0.34})Se_2$ was approximately 0.87, and the diode and photovoltaic parameters were also improved. At this condition, the doping concentration and junction depth were $7\times10^{15}cm^{-3}$ and approximately 650 nm, respectively. The current collection efficiency in red light and longer wavelengths was improved in the sturdy junction. The efficiency of $CdS/Cu(In,Ga)Se_2$ solar cell was 13.4% when the composition of CIGS film was $Cu_{0.87}(In_{0.66}Ga_{0.34})Se_2$.

Keywords: solar cell, CIGS, Cu content, doping concentration, selenide source

1. INTRODUCTION

$Cu(In,Ga)Se_2$ (CIGS), with a direct band gap and a high absorption coefficient, is a promising absorbing material for polycrystalline thin film solar cells. Employing the co-evaporation of Cu, In, Ga, and Se elements with a three-stage process, CIGS solar cells have demonstrated high potential in photovoltaics with laboratory cell efficiencies exceeding 18%.[1-3] Since binary selenides such as Cu_2Se, In_2Se_3, and Ga_2Se_3 have higher vapor pressures than elemental sources such as Cu, In, and Ga elements, they have been used as evaporation sources to deposit CIGS films.

Due to difficulties in controlling the stoichiometry of CIGS films by the evaporation of selenide sources, few studies have been reported. The application of binary selenide sources has been reported with regard to $CuInSe_2$ and $Cu(In,Ga)Se_2$.[4-6] Thus far, the highest obtained CIGS cell efficiencies have been below 12% for CIGS cells prepared by the evaporation of binary selenides. The compositional variation in CIGS film has an important effect on the device performance.[7,8] However, no systematic investigation on the effect of Cu content has been reported, particularly for CIGS cells fabricated using binary selenide sources such as In_2Se_3, Ga_2Se_3, or Cu_2Se. In this work, the Cu content in the CIGS layer was varied by evaporating binary selenide powders. In addition, the photovoltaic properties of a cell utilizing the CIGS layer were systematically studied as a function of Cu content, which significantly affects the doping concentration and junction depth in CIGS films.

*Corresponding author: btahn@kaist.ac.kr

2. EXPERIMENTAL

The substrate used in our experiment is a soda lime glass with a 1 μm thick Mo layer deposited by dc-magnetron sputtering at room temperature. A CIGS absorber layer was deposited by a three-stage process using the binary selenide sources In_2Se_3, Ga_2Se_3, Cu_2Se, and Se.[6] In the first stage, In_2Se_3, Ga_2Se_3, and Se elements were evaporated and deposited on the Mo/glass substrate at 350°C to form an $(In,Ga)_2Se_3$ layer with a thickness of 1 μm. In the second stage, Cu_2Se was evaporated on the $(In,Ga)_2Se_3$ layer at 525°C to form CIGS film *in-situ*. The second stage proceeded until the overall CIGS film became Cu-rich, which caused grain size increases above 2 μm. The CIGS films were then annealed at 525°C for 10 min in a Se environment in the same evaporation chamber. In the third stage, In_2Se_3, Ga_2Se, and Se elements were evaporated on the CIGS layer at 525°C with various deposition times in order to control the Cu content in the layer, converting the CIGS layer into p-type. The resulting thickness of the CIGS layer was typically in the range of 1.8 to 2.0 μm. The as-deposited CIGS material was characterized using scanning electron microscopy (SEM) and Auger electron spectroscopy (AES).

Solar cells with an Al/n-ZnO/i-ZnO/CdS/CIGS/Mo/glass structure were fabricated with the following process. An 80-

nm thick CdS buffer layer was grown on the CIGS layer by chemical bath deposition (CBD). 50-nm thick i-ZnO and 0.95-μm thick n-ZnO layers were deposited on the CdS layer by RF magnetron sputtering as a transparent conducting oxide. The resistivities of the i-ZnO and n-ZnO layers were ~10^6 and 5×10^{-4} Ω·cm, respectively. The optical transmittance of the ZnO layer was above 85%. Finally, an Al grid was deposited as a current collector on the ZnO by e-beam evaporation. The solar cells were analysed with electron-beam induced current (EBIC), current-voltage (J-V), and spectral quantum efficiency (QE) measurements. The cell performance was evaluated under an AM 1.5 at 100 mW/cm^2 illumination.

3. RESULTS AND DISCUSSION

Figure 1 shows the AES depth profiles of Cu content in the $Cu_x(In_{0.66}Ga_{0.34})Se_2$ films with various third-stage evaporation times. The profiling was conducted before CdS deposition. At 525°C, Cu is the most mobile atom in the CIGS films and the element Cu readily diffuses and spread out from the middle layer to both sides. First, the Cu content in the bulk is lowered as the third-stage evaporation time increases. The bulk region in our analysis is the region where the Cu concentration as a function of depth is nearly constant. For example, the bulk region in the sample with 1 min evaporation is between 1000 to 2000 nm, as seen in Fig. 1. The average Cu contents in the bulk region after 1, 3, 5, and 8 min of evaporation time are 0.95, 0.89, 0.85, and 0.83, respectively. Second, when the evaporation time is less than 5 min, the Cu content at the surface is slightly lower compared to that in the bulk. In Cu-rich CIGS films, atoms such as Cu, In, and Ga can diffuse easily,[9] and thus, the Cu content in the CIGS film does not show a noticeable difference between surface and bulk when the third-stage time is short. Third, the Cu content near the surface is remarkably lower than that in the bulk after 8 min of evaporation.

CIGS solar cells with a structure of Al/n-ZnO/i-ZnO/CdS/CIGS/Mo/glass were fabricated using the CIGS films, and a typical cross-section of the cell is shown in Fig. 2. ZnO, CIGS, and Mo on the glass substrate are clearly seen. However, the CdS layer on the CIGS layer can be distinguished only at higher magnification. Using the cells, the junction and photovoltaic properties were analysed.

The doping concentration in the bulk was determined from the C-V measurement assuming that the CIGS film has an abrupt step junction, and the C-V behaviour is described by the following equations.

$$\phi_i - V_a = -q\varepsilon_s N_a / 2C^2 \quad (1)$$

$$N_a = -2/q\varepsilon_s \, [d(1/C^2)/dV], \quad (2)$$

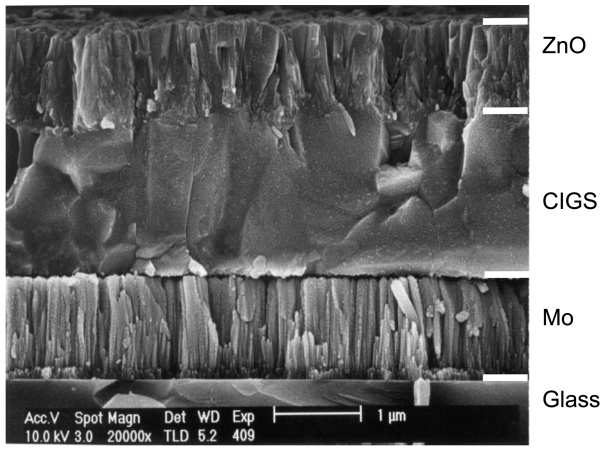

Fig. 2. SEM cross section of CIGS cell with an n-ZnO/i-ZnO/CdS/CIGS/Mo/glass structure.

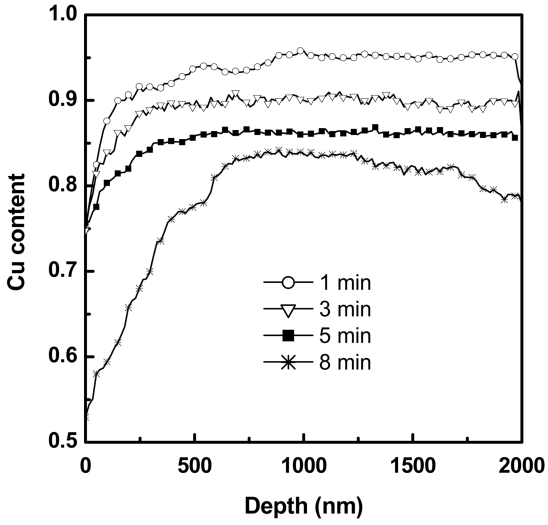

Fig. 1. AES depth profiles of the Cu content in a $Cu_x(In_{0.66}Ga_{0.34})Se_2$ absorber with various third-stage evaporation times.

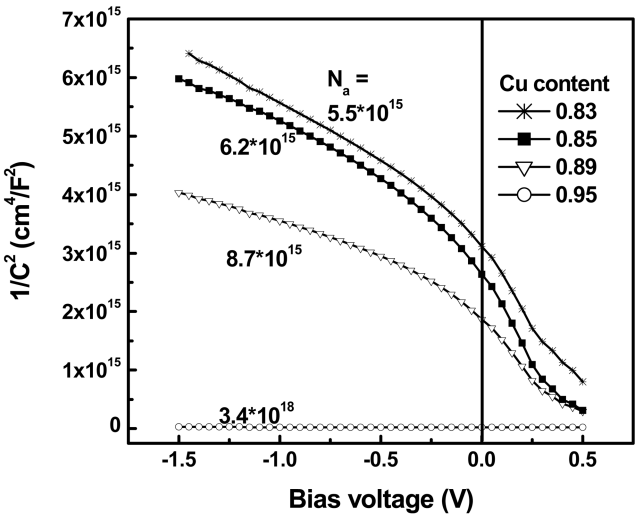

Fig. 3. $1/C^2$ versus bias voltage of the CdS/$Cu_x(In_{0.66}Ga_{0.34})Se_2$ junction with various Cu contents.

where ϕ_i is the built-in potential, V_a the applied voltage, ε_s the permittivity of CIGS ($13.5\varepsilon_o$), and N_a the acceptor concentration.

Figure 3 shows the $1/C^2$ versus bias voltage of the n-CdS/p-CIGS cells with various Cu contents in the CIGS layer. The CV measurement was carried out at 1 MHz frequency. In the curves, the plot is expected to be straight in the uniformly doped bulk region. For the composition with $x = 0.95$, the $1/C^2$ value is too small to be seen in the figure. The $1/C^2$ values for $x = 0.95$ at -1.5 and zero V are 2.8×10^3 and $2.1 \times 10^{13} cm^4/F^2$, respectively. The bulk doping concentrations in the CIGS film with Cu content of 0.95, 0.89, 0.85, and 0.83 are 3.4×10^{18}, 8.7×10^{15}, 6.2×10^{15}, and 5.5×10^{15} cm^{-3}, respectively. The doping concentration of $3.4 \times 10^{18} cm^{-3}$ is possible since it is known that the maximum doping concentration of CIS is about $1 \times 10^{19} cm^{-3}$.[10] However, adding Ga to CIS causes an increase of the doping concentration, so an even higher doping level can be obtained.[10] In Fig. 3, the doping concentration is lowered as the Cu content decreases.

From equation (2), the doping concentration is inversely proportional to the slope of the curves in Fig. 3. The $1/C^2$-V slope is nearly constant in the bias voltage of -1 to -0.5 V, and it is increased as the bias voltage approaches zero bias. Therefore, the doping concentration is constant in the bias voltage of -1 to 0.5 V and is decreased as the bias voltage approaches zero bias. The approximate Cu doping concentrations at the zero bias voltage are 3×10^{18}, 5×10^{15}, 3×10^{15}, and $2 \times 10^{15} cm^{-3}$, respectively. The junction depth can be estimated from the equation $x_d = (2\varepsilon_s \phi_i / qN_a)^{1/2}$, where $\varepsilon_s = 13.5\varepsilon_o$, ϕ_i is the built-in potential and N_a is the doping concentration at the depletion edge. The ϕ_i value was determined from the cross point on the x-axis by extrapolating the slope of the $1/C^2$-V curves in the range of -1 to -0.5 V, where the doping concentration is constant. The junction depths for 1, 3, 5, and 8 min of evaporation are approximately 50, 550, 710, and 810 nm, respectively.

An electron beam was irradiated through the cross-section of the ZnO/CdS/CIGS cell, and the e-beam induced current was measured. Figure 4 shows an EBIC profile superimposed on SEM cross-section images of the CIGS cells with the Cu content of (a) 0.95, (b) 0.89, (c) 0.85, and (d) 0.83. The cleaved surface for electron beam exposure was unpolished. The surface roughness might affect the EBIC signal, but the overall current profile was slightly affected by the roughness. The white bold bars in Fig. 4 are the demarcations of Mo/CIGS and CdS/ZnO. Since the CdS layer is too thin, the demarcation at the CdS/ZnO can be considered as the CIGS/CdS interface.

In Fig. 4a, a sharp peak is positioned near the CdS/CIGS interface. The peak position moves toward the CIGS bulk as the Cu content decreases (Figs. 4b and 4c), qualitatively indicating that the junction depth has increased. The positions of the peaks in the CIGS layer with Cu content of 0.95, 0.89, 0.85, and 0.83 are 0, 600, 800, and 1100 nm, respectively, from the CdS/CIGS interface. The broad peak in the CIGS layer with Cu content of less than 0.89 indicates that the excited charges are easily separated throughout the absorbing layer. Note that the peak width is the broadest in Fig. 4c, indicating that the width of the effective space charge is largest. In this case the shunt resistance is large and the series resistance is small, as we will see later. For Cu = 0.83 (Fig. 4d), the current collection is particularly low

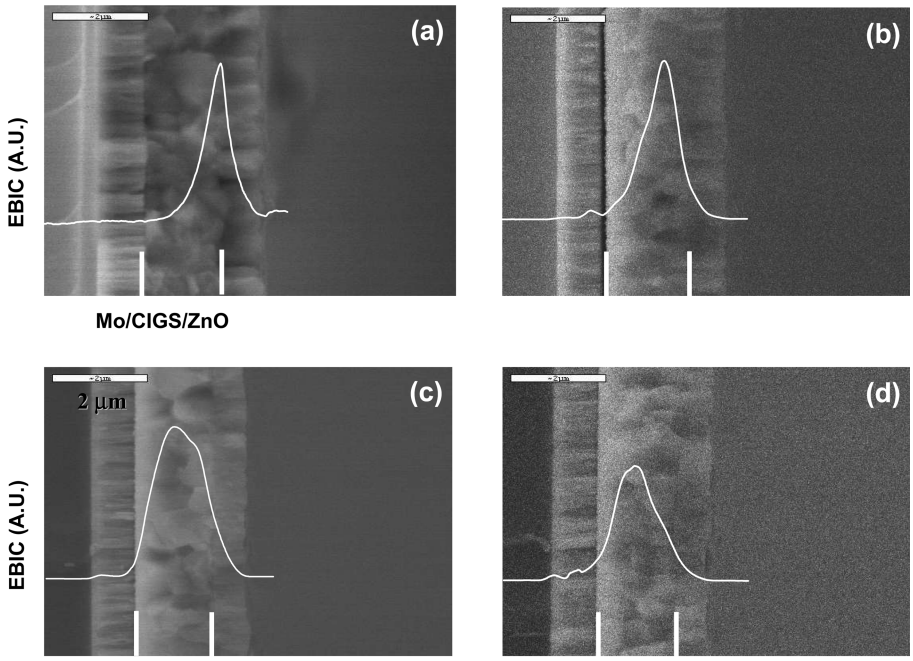

Fig. 4. EBIC responses of CdS/ $Cu_x(In_{0.66}Ga_{0.34})Se_2$ junction with Cu content of (a) 0.95, (b) 0.89, (c) 0.85, and (d) 0.83.

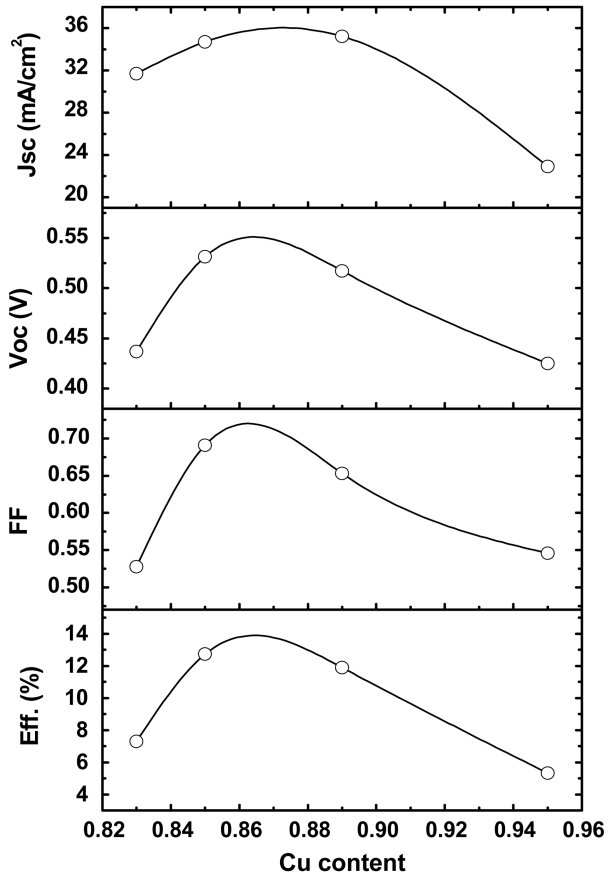

Fig. 5. Photovoltaic cell parameters of CdS/ $Cu_x(In_{0.66}Ga_{0.34})Se_2$ solar cells as a function of Cu content.

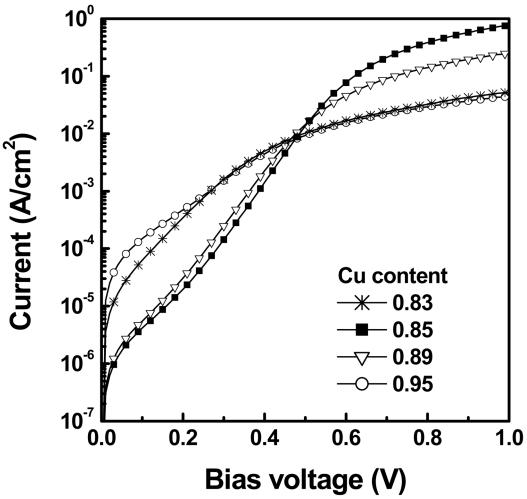

Fig. 6. Dark J-V curves of CdS/ $Cu_x(In_{0.66}Ga_{0.34})Se_2$ solar cells with various Cu contents.

due to small built-in potential because the doping concentration is too low (2×10^{15} /cm^{-3} near surface).

Figure 5 shows the photovoltaic parameters of the CIGS solar cells with an active area of 0.21 cm^2 (total area = 0.26 cm^2) as a function of the bulk Cu content. As the Cu content decreases from 0.95 to 0.87, the current density (J_{sc}), open circuit voltage (V_{oc}), and fill factor (FF) are greatly increased, resulting in an increase of cell conversion efficiency. However, the values of these parameters become smaller when the Cu content is 0.83. Note that the V_{oc} and FF drop fast as the Cu content changes from 0.85 to 0.83, while the I_{sc} does drop slowly. From the figure it can be seen that the best result can be obtained when the Cu content is near 0.87, where the doping concentration is about 7×10^{15} and the junction depth is approximately 650 nm.

Our experimental results with EBIC and light absorption indicate that the junction depth with best result is approximately 650 nm, where the Cu content is about 0.87. However, the current collection profile shown by EBIC may be different from the collection profile in terms of light absorption. For example, the absorption coefficient of a 800-nm wavelength is 10^5 cm^{-3} in CIGS so that the penetration depth of CIGS is about 100 nm, which is closer to the surface. It was reported that the Cu poor composition allows penetration of light into deeper CIGS bulk.[7,11] However, the penetration depth will not be changed significantly. This suggests that a sturdy pn junction that effectively collects excited electrons and holes is much more important than the penetration depth of sunlight.

The shunt resistances, R_{sh}, of the cells with Cu content of 0.95, 0.89, 0.85, and 0.83 are 200, 750, 1800, and 200 $\Omega\cdot cm^2$, respectively. The series resistances, R_s, are 0.7, 0.75, 0.35, and 1.2 $\Omega\cdot cm^2$, respectively. Note that the cell with a Cu content of 0.85 has the largest R_{sh} and the lowest R_s, indicating that the content makes a sturdy pn junction. The cell with Cu = 0.95 has a small R_{sh} due to heavy doping, while the cell with Cu = 0.83 has a small R_{sh} due to a low doping concentration where the junction potential barrier is small.

Figure 6 shows dark J-V curves of the CIGS cells with various Cu contents in the CIGS layer. The diode characteristic can be expressed as $J = J_o\cdot\exp(qV_a/AkT)$, where V_a is the bias voltage, A the diode ideality factor, and k the Boltzmann constant. The cells with Cu = 0.95 and 0.83 show high saturation currents, while the cells with Cu = 0.89 and 0.85 show low saturation currents. A low saturation current is an indication of large R_{sh} and high V_{oc}. The diode ideality factors for Cu = 0.89 and 0.85 are 1.67 and 1.7, respectively, indicating that the recombination mechanism in the cells is a combination of space-charge recombination (A = 2) and thermionic emission of charge carriers over the barrier (A = 1). Note that the cell with Cu = 0.85 shows a high current at a bias voltage of 1 V, which is an indication of low R_s. The diode factor of record efficiency cell is reported as 1.3~1.35.[1]

Figure 7 shows the spectral quantum efficiency of CdS/ CIGS solar cells with various Cu contents in the CIGS layer. The quantum efficiency is directly related to the collection

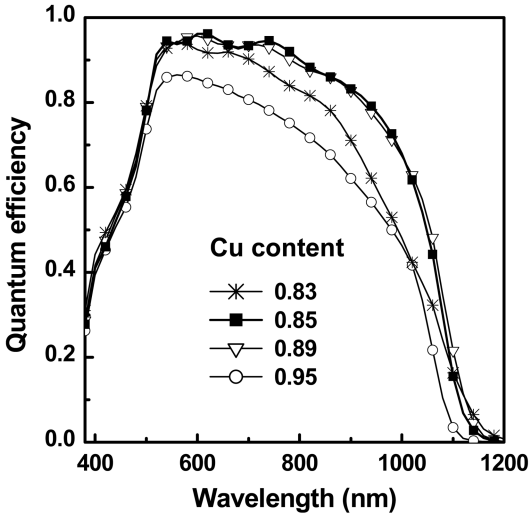

Fig. 7. Spectral quantum efficiency of CdS/$Cu_x(In_{0.66}Ga_{0.34})Se_2$ solar cells with various Cu contents.

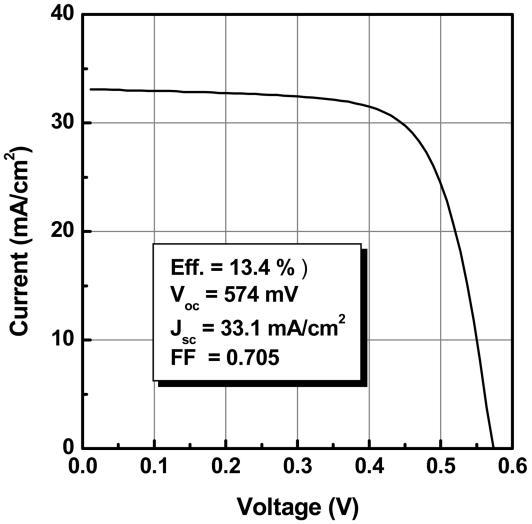

Fig. 8. 13.4% efficiency was achieved in the CdS/$Cu_x(In_{0.66}Ga_{0.34})Se_2$ with binary selenide sources.

efficiency of the specific photon energy. The cell with Cu = 0.95 exhibits low efficiency throughout the visible wavelength range. This is simply due to poor charge collection with a narrow space-charge region. The cells with Cu = 0.89 and 0.85 show a good spectral response. However, the efficiency in the red and longer wavelength range decreases, suggesting that further improvement is necessary in the charge collection at the long wavelength. To this end, it is necessary to improve the microstructure of the CIGS layer; this, however, is beyond the scope of the present paper. The cell with Cu = 0.83 shows a good response near blue wavelength, but shows a much poorer response in the red and longer wavelength compared to cells with Cu = 0.89 and 0.85.

From the above results, the most appropriate level of Cu content in the CIGS layer is considered to be 0.87. Figure 8 shows the J-V curve of the CIGS solar cells with the best efficiency. A cell efficiency of 13.4% with V_{oc} = 574 mV, J_{sc} = 33.1 mA/cm^2, and FF = 0.705 was realized from the cell with an active area of 0.21cm^2. While the efficiency is significantly improved compared to the reported value, it is still lower than that fabricated from elemental sources.[6,7] As discussed in the spectral quantum efficiency analysis (Fig. 7), it is necessary to further improve the microstructure of CIGS bulk film in order to achieve higher conversion efficiency. Recently, Kim et al. reported that the Se flux in the third-stage critically affects the morphology of CIGS layer that is prepared from elemental sources.[12] By applying the technique we believe that the microstructure can be further improved and the higher cell efficiency can be obtained.

4. CONCLUSIONS

A Cu(In,Ga)Se_2 layer was fabricated by a three-stage process involving the co-evaporation of the binary selenides including $Cu_{2-x}Se$, In_2Se_3, and Ga_2Se_3. As the Cu content decreased from 0.95 to 0.83, the doping concentration in the bulk layer was lowered from 10^{19} to 5×10^{15} cm^{-3}. The surface Cu content was slightly lower than that in the bulk when the Cu content was high, but it was significantly lower when the Cu content was 0.83. The CdS/CIGS cell with Cu = 0.95 had a weak junction due to heavy doping, while the cell with Cu = 0.83 had a weak junction due to very low doping. The sturdiest junction was realized when the Cu content in the $Cu_x(Ga_{0.66}Ga_{0.34})Se_2$ was approximately 0.87, where large R_{sh}, small R_s, and low saturation current were possible. At this condition, the bulk doping concentration and junction depth were approximately 7×10^{15} cm^{-3} and 650 nm, respectively. The highest efficiency of 13.4% with V_{oc} = 574 mV, J_{sc} = 33.1 mA/cm^2, and FF = 0.705 was achieved in the CdS/CIGS cell with an active area of 0.21cm^2 by using Cu_2Se, In_2Se_3, and Ga_2Se_3 as evaporation sources.

ACKNOWLEDGMENT

This work was supported by the Korea Research Foundation Grant (KRF-2005-005-J09702).

REFERENCES

1. M. A. Contreras, K. Ramanathan, J. AbuShama, F. Hasoon, D. L. Young, B. Egaas, and R. Noufi, *Prog. Photovolt. Res. Appl.* **13**, 209 (2005).
2. T. Negami, Y. Hashimoto, and S. Nishiwaki, *Sol. Engergy Mater. Sol. Cells* **67**, 331 (2001) .
3. Y. Hagiwara, T. Nakada, and A. Kunioka, *Sol. Engergy Mater. Sol. Cells* **67**, 267 (2001).

4. S. C. Park, D. Y. Lee, B. T. Ahn, K. H. Yoon, and J. S. Song, *Sol. Energy Mater. Sol. Cells* **69**, 99 (2001).
5. D. Y. Lee, J. H. Yun, K. H. Yoon, and B. T. Ahn, *Thin Solid Films* **410**, 171 (2002).
6. D. Y. Lee, B. T. Ahn, K. H. Yoon, and J. S. Song, *Sol. Energy Mater. Sol. Cells* **75**, 73 (2003).
7. D. Schmid, M. Ruckh, F. Grunwald, and H. W. Schock, *J. Appl. Phys.* **73**, 2902 (1993).
8. A. J. Nelson, A. M. Gabor, M. A. Contreras, J. R. Tuttle, R. Noufi, P. E. Sobol, P. Asoka-Kumar, and K. G. Lynn, *J. Appl. Phys.* **78**, 269 (1995).
9. M. Nishitani, T. Nagami, and T. Wada, *Thin Solid Films* **258**, 313 (1995).
10. S. B. Zhang, S.-H. Wei, and A. Zunger, *J. Appl. Phys.* **83**, 3192 (1998).
11. S. H. Han, F. S. Hasoon, H. A. Al-Thani, A. M. Hermann, and D. H. Levi, *J. Phys. Chem. Solids* **66**, 1895 (2005).
12. K. H. Kim, K. H. Yoon, J. H. Yun, and B. T. Ahn, *Electrochem. Solid-State Lett.* **9**, A382 (2006).